

GaAs on (001) Si templates for near-infrared InP quantum dot lasers

Cite as: J. Appl. Phys. **132**, 193103 (2022); <https://doi.org/10.1063/5.0124664>

Submitted: 07 September 2022 • Accepted: 30 October 2022 • Published Online: 17 November 2022

 Jie Huang,  Qi Lin,  Wei Luo, et al.



View Online



Export Citation



CrossMark

ARTICLES YOU MAY BE INTERESTED IN

[Effects of B and In on the band structure of BGa\(In\)As alloys](#)

Journal of Applied Physics **132**, 193104 (2022); <https://doi.org/10.1063/5.0125109>

[Metasurfaces for photonic devices](#)

Journal of Applied Physics **132**, 190401 (2022); <https://doi.org/10.1063/5.0131810>

[THz detection and amplification using plasmonic field effect transistors driven by DC drain currents](#)

Journal of Applied Physics **132**, 193102 (2022); <https://doi.org/10.1063/5.0128496>



APL Quantum

CALL FOR APPLICANTS

Seeking Editor-in-Chief

GaAs on (001) Si templates for near-infrared InP quantum dot lasers

Cite as: J. Appl. Phys. **132**, 193103 (2022); doi: [10.1063/5.0124664](https://doi.org/10.1063/5.0124664)

Submitted: 7 September 2022 · Accepted: 30 October 2022 ·

Published Online: 17 November 2022



Jie Huang,  Qi Lin,  Wei Luo,  Liying Lin,  and Kei May Lau^{a)} 

AFFILIATIONS

Department of Electronic and Computer Engineering, Hong Kong University of Science and Technology, Clear Water Bay, Kowloon, Hong Kong

^{a)}Author to whom correspondence should be addressed: eeekmlau@ust.hk

ABSTRACT

We investigated the effects of thermal cycle annealing (TCA) at high temperatures on the defect density and morphology of GaAs epilayers grown on (001) Si substrates. Several types of TCA combined with dislocation filter layers (DFLs) were introduced to reduce the defect densities in the GaAs grown on Si substrates. Plan-view transmission electron microscopy shows that the defect density of a 2.7 μm -thick GaAs/Si template with optimized TCA and DFLs is $1.4 \times 10^7 \text{ cm}^{-2}$, lower than a 1.1 μm -thick GaAs/Si template by a factor of 40. The surface roughness of the optimized GaAs/Si template is 1.3 nm after insertion of the DFLs. Additionally, optically pumped InP quantum dot micro-disk lasers (MDLs) were fabricated on these GaAs/Si templates to evaluate the template quality. Room-temperature continuous-wave lasing of 1.5 μm -diameter MDLs was observed, with ultralow lasing thresholds ranging from 0.5 to 2 μW .

Published under an exclusive license by AIP Publishing. <https://doi.org/10.1063/5.0124664>

I. INTRODUCTION

Over the years, Si has been the backbone material in conventional electronic circuits for data processing.¹ Recently, Si-based photonic integrated circuits (PICs) have gained increasing attention because of their advantages in power consumption, high speed, and large bandwidth capability.² III-V compound-based devices with superior optical properties on (001) Si make III-V/Si hetero-epitaxy highly desirable for monolithic integration.³ III-V quantum dot (QD) lasers directly grown on Si have shown good performance in temperature stability and gain bandwidth due to discrete distribution and strong carrier confinement.^{4,5} InP QD lasers grown on GaAs emitting at the red and near-infrared (NIR) range are important for underwater communication and molecular diagnostics.^{6,7} InP QD lasers lasing at 730 nm have been demonstrated on (001) GaAs substrates with 10°-toward the (111)A direction.⁸ Realization of PICs on Si in the red and NIR regime using InP QD lasers grown on Si is a promising direction of investigation. However, the epitaxy of GaAs on Si faces many challenges including large lattice mismatch (4%), polar/non-polar interface, and a large difference in thermal expansion coefficient between GaAs and Si. A high density of crystalline defects such as threading dislocations (TDs) and stacking faults (SFs) formed at the GaAs/Si hetero-interface significantly degrades the lifetime and reliability of the devices.⁹ The

polar/non-polar interface between GaAs and Si gives rise to the generation of anti-phase boundaries (APBs), which are another type of defect in the GaAs layer degrading device performance. Traditionally, offcut Si substrates from the exact (001) orientation by 2°–4° toward the [110] direction have been utilized to minimize the formation of APBs during the growth of III-V materials on Si.^{10–14} APB-free GaAs was obtained on standard nominal Si (001) wafers due to the formation of double step by annealing Si substrate at high temperature under H₂.¹⁵ Meanwhile, growth approaches including strained layer superlattices (SLSs), thermal cycle annealing (TCA), and compositionally graded buffers have been introduced to grow highly mismatched materials on different substrates so as to reduce the threading dislocation densities (TDDs).^{16–21}

In this work, we report APB-free and smooth GaAs films grown on commercial nominal (001) silicon (~0.5° offcut with random orientation) in a metalorganic chemical vapor deposition (MOCVD) system at a low growth pressure of 100 mbar. We investigated the effects of TCA and InGaAs/GaAs SLSs on the defect density and surface roughness of the GaAs/Si templates. Based on the optimized GaAs/Si templates, optically pumped InP QD micro-disk lasers (MDLs) were fabricated on the templates, with the lowest threshold of 0.5 μW in continuous-wave (CW) mode at room temperature (RT).

II. EXPERIMENTAL PROCEDURE

The growth of the GaAs/Si templates was performed in an AIXTRON Close Coupled Showerhead (CCS) MOCVD system equipped with a LayTec Epicurve-TT system for reflectance monitoring. Prior to growth, a 4-in. Si (001) wafer was cleaned in boiling $\text{NH}_3\text{OH}:\text{H}_2\text{O}_2:\text{H}_2\text{O}$ (1:1:5) solution for 10 min and deoxidized by 1% HF solution for 90 s. The wafer was then loaded into the MOCVD chamber and annealed in a pure H_2 ambient at 850 °C for 15 min to deoxidize and form bi-atomic terraces on the Si surface. A uniform GaAs nucleation layer (~ 10 nm) was initiated with GaAs islands first at 400 °C, with a V/III ratio of 30, using triethylgallium (TEGa) and tertiarybutylarsine (TBA) as precursors. Subsequently, two layers of GaAs with a total thickness of 1 μm were grown at 510 and 560 °C, respectively. The full width at half-maximum (FWHM) of the x-ray diffraction (XRD) rocking curves of the 1 μm -thick GaAs/Si template is 600 arcsec. Next, the 4-in. as-grown 1 μm -thick GaAs/Si template without TCA was cleaved into several pieces (2×2 cm²) for subsequent experiments with TCA and dislocation filter layers (DFLs) growth. Three types of TCA were experimented on the 1 μm -thick GaAs/Si templates to reduce the crystalline defects, followed by two types of $\text{In}_x\text{Ga}_{1-x}\text{As}/\text{GaAs}$ SLSs insertion for further reduction in TD. The InP QD MDL structure was grown on the different GaAs/Si templates in an AIXTRON 200/4 MOCVD system. The laser structure begins with a 500 nm $\text{Al}_{0.3}\text{Ga}_{0.7}\text{As}$ layer grown at 710 °C to serve as the sacrificial layer in forming a pillar of the MDLs. Then, a 110 nm $(\text{Al}_{0.55}\text{Ga})_{0.52}\text{In}_{0.48}\text{P}$ cladding layer was grown at the same temperature, followed by 3.2 ML InP QDs and 10 nm $(\text{Al}_{0.1}\text{Ga})_{0.52}\text{In}_{0.48}\text{P}$ cap layer grown at 690 °C. Finally, a 110 nm $(\text{Al}_{0.55}\text{Ga})_{0.52}\text{In}_{0.48}\text{P}$ cladding layer was grown at 710 °C. Using dispersed silica beads as the hard mask, inductively coupled plasma (ICP) dry etching was conducted subsequently to fabricate a cylindrical pillar. After that, the $\text{Al}_{0.3}\text{Ga}_{0.7}\text{As}$ pedestal was formed by immersing the sample in a $\text{H}_3\text{PO}_4:\text{H}_2\text{O}_2:\text{H}_2\text{O}$ (3:1:30) solution for 60 s.²²

III. RESULTS AND DISCUSSION

The surface morphology of the as-grown GaAs/Si templates was assessed by atomic force microscopy (AFM). As shown in Fig. 1, the surface roughness of a 1 μm -thick GaAs/Si sample is 1.26 nm, root-mean square (RMS) of the $10 \times 10 \mu\text{m}^2$ AFM image. Step flow and several SFs along the $\langle 110 \rangle$ direction can be observed on the surface of GaAs with irregular undulation.

The detailed TCA conditions used in our study are described in Table I, and the corresponding templates are labeled as S_1 – S_3 . For sample S_1 , four cycles of TCA were performed on the GaAs/Si template with temperature cycling between 330 (5 min) and 680 °C (5 min), after which a 100 nm GaAs layer was grown on top at 560 °C. Sample S_2 was heated to 740 °C under an arsenic overpressure environment, held at that temperature for 4 min, and then cooled down to 330 °C for four cycles. Different from samples S_1 and S_2 , two sets of TCA were performed on sample S_3 . The first set of TCA was the same as that carried out on sample S_1 . The 350 nm GaAs layer grown at 650 °C was intended to act as an intermediate layer to avoid decomposition of GaAs during the second TCA at high

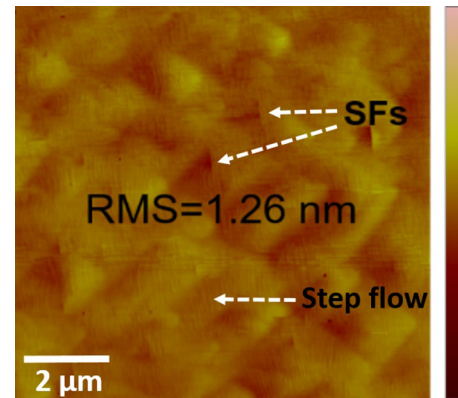


FIG. 1. $10 \times 10 \mu\text{m}^2$ AFM image of a 1 μm -thick GaAs/Si template with step flow and SFs. The RMS value is 1.26 nm. The color scale is 30 nm.

temperature. The second set of TCA was performed on sample S_3 with a maximum temperature of 730 °C. The reduction in the FWHM of the XRD rocking curves of the GaAs/Si template from 600 to 382 arcsec proves that the crystalline quality of the GaAs was improved significantly by the TCA technique. The FWHM of the XRD rocking curves of the GaAs/Si templates decreased from 382 to 198 arcsec as the temperature gap and the number of cycles in the TCA increased.

The surface morphology of sample S_1 illustrated in Fig. 2(a) shows a low surface roughness of 1.1 nm, and several SFs can be observed on the surface of the sample. From the AFM image of sample S_2 shown in Fig. 2(b), the SF density decreased significantly with the increase in the annealing temperature. However, the GaAs surface degraded dramatically when the maximum annealing temperature reached 740 °C, which is consistent with the report from Shang *et al.*,²³ and many pits formed on the GaAs surface due to

TABLE I. Samples with different TCA conditions.

| Sample no. | TCA condition | FWHM (arcsec) | Thickness (μm) |
|------------|--|---------------|-----------------------------|
| S_1 | 4 cycles TCA between 680 and 330 °C + 100 nm 560 °C GaAs | 382 | 1.1 |
| S_2 | 4 cycles TCA between 740 and 330 °C + 100 nm 560 °C GaAs | 323 | 1.1 |
| S_3 | 4 cycles TCA between 680 and 330 °C + 150 nm 560 °C GaAs layer (first TCA) 350 nm 650 °C GaAs layer + 4 cycles TCA between 730 and 330 °C + 100 nm 560 °C GaAs (second TCA) | 198 | 1.6 |

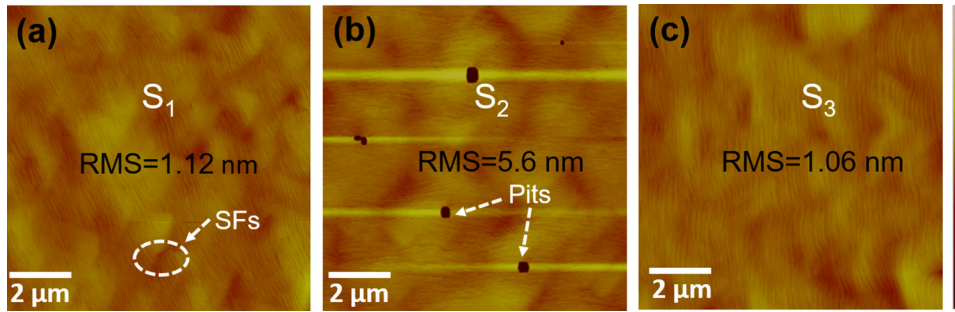


FIG. 2. $10 \times 10 \mu\text{m}^2$ AFM images of sample (a) S_1 with SFs, (b) S_2 with pits, and (c) S_3 with smooth surface. The RMS values for these three samples are 1.12, 5.6, and 1.06 nm, respectively. The color scale is 30 nm.

its decomposition at high temperature. On top of sample S_3 , another 100 nm GaAs layer was grown at 560 °C after the second four cycles. Based on the optimization of the TCA conditions on sample S_3 , a smooth surface with a clear step flow was achieved for the GaAs/Si template, with a surface roughness of 1.06 nm, as illustrated in Fig. 2(c). The surface morphology of sample S_3 was improved by introducing the GaAs intermediate layer at 650 °C and the second four cycles of TCA at 730 °C.

As illustrated in Figs. 3(a) and 3(b), two types of InGaAs/GaAs SLSs acting as DFLs were grown on different GaAs/Si templates at 510 °C, and the corresponding structures are labeled as T_1 and T_2 . One set of InGaAs/GaAs DFLs consists of 10 periods of 9.6 nm $\text{In}_{0.158}\text{GaAs}/12$ nm GaAs, and the thickness of the GaAs spacer in template T_1 is 400 nm. To decrease the total thickness of GaAs buffer, a 280 nm GaAs spacer was grown in T_2 . Figures 3(c) and 3(d) present the surface morphology of samples T_1 and T_2 , respectively. The surface roughness of the two templates is 1.76 and 1.3 nm measured from two $10 \times 10 \mu\text{m}^2$ AFM images, and the step flow formed on sample T_2 is more apparent than that on sample

T_1 . The surface roughness of these two templates was increased due to the two sets of 10 period SLSs insertion.

Figures 4(a) and 4(b) show plan-view transmission electron microscopy (PV-TEM) images of samples T_1 and T_2 , respectively. The average defect density of samples T_1 and T_2 obtained from statistical data over an area of $300 \mu\text{m}^2$ is counted to be 6.4×10^7 and $1.4 \times 10^7 \text{cm}^{-2}$, respectively. Figure 4(c) presents the surface roughness and defect density of different GaAs/Si templates as a function of buffer thickness. A lower defect density of $1.4 \times 10^7 \text{cm}^{-2}$ and a smooth surface with an RMS value of 1.3 nm were obtained on sample T_2 with a total GaAs buffer thickness of 2.7 μm , showing a significant reduction by a factor of 40 compared to sample S_1 .

Cross-sectional TEM (X-TEM) images of samples T_1 and T_2 are depicted in Figs. 5(a) and 5(b), respectively. A high density of TDs and SFs generated at the GaAs/Si hetero-interface propagated toward the interface between the first SLSs and GaAs without obvious interruption, as shown in Fig. 5(a). The propagation of some TDs and SFs was bent inside the first SLSs, and their glide direction was changed to the (001) plane. However, the rest of TDs

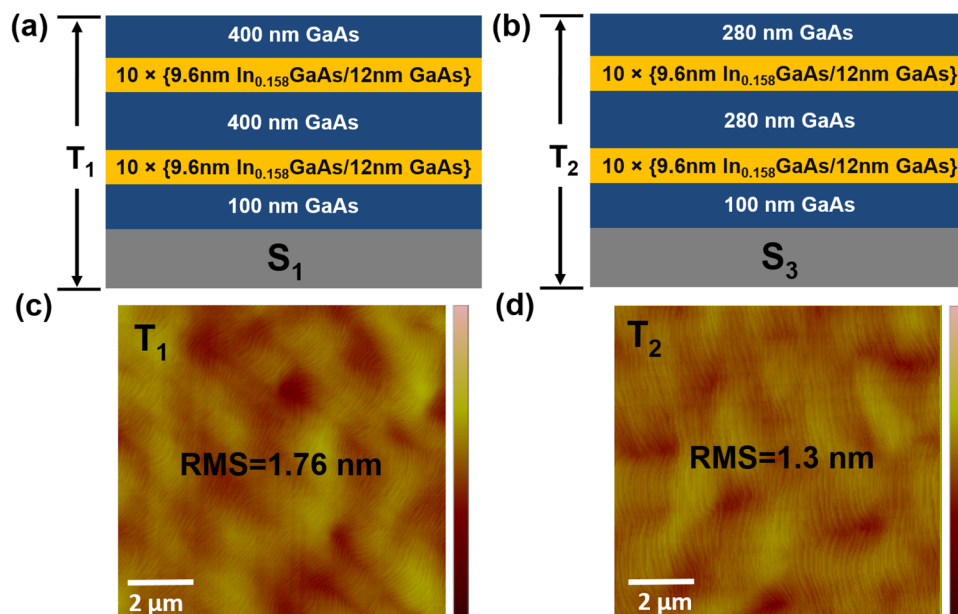


FIG. 3. Schematic diagrams of samples (a) T_1 and (b) T_2 . Both T_1 and T_2 contain two sets of 10 periods of 9.6 nm $\text{In}_{0.158}\text{GaAs}/12$ nm GaAs SLSs, and the spacer thicknesses in T_1 and T_2 are 400 and 280 nm, respectively. $10 \times 10 \mu\text{m}^2$ AFM images of sample (c) T_1 and (d) T_2 . RMS values for these two samples are 1.76 and 1.3 nm, respectively. The color scale is 30 nm.

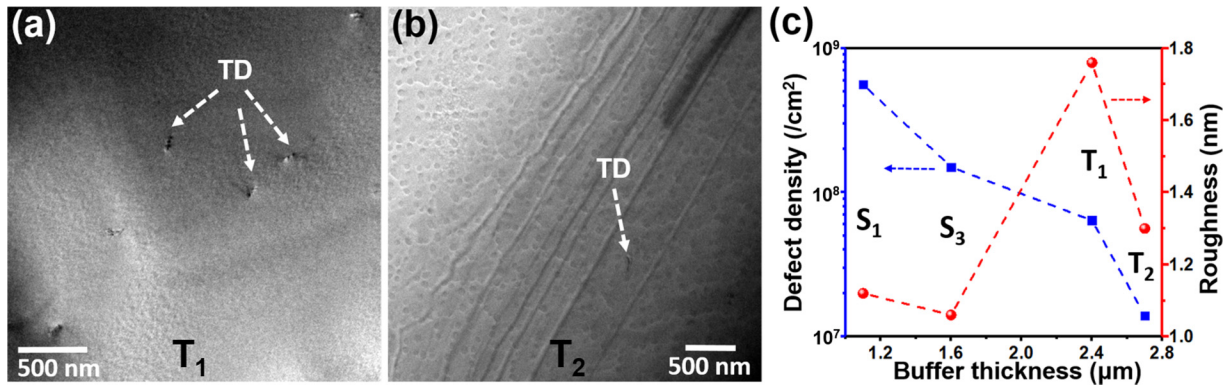


FIG. 4. PV-TEM images of samples (a) T_1 and (b) T_2 . (c) Surface roughness and defect density of the GaAs/Si templates vs buffer thicknesses. Defect density decreased from 5.8×10^8 (S_1) to 1.4×10^7 cm^{-2} (T_2), and T_2 has a smooth surface with an RMS value of 1.3 nm.

could not be blocked by the DFLs. They moved up through the epilayers and reached the top surface of the GaAs, as evidenced in Fig. 5(a). Since the threading dislocation density (TDD) was still very high after the TCA, the DFLs could not bend all defects into the (001) plane of the SLSs with the finite influence of strain on the defects. Therefore, the remaining defects propagated up to the top surface of the GaAs.

Compared to sample T_1 , the interaction and annihilation of defects took place more prominently in the GaAs epilayer between the first SLSs and GaAs/Si interface in sample T_2 during the TCA due to the dislocation movement under high temperature and thermal stress conditions.^{24,25} So, the TDD at the GaAs/Si interface in sample T_2 is lower than that in sample T_1 . In general, annealing at high temperature allows sufficient strain relaxation in GaAs film, which promotes the movement of dislocations.²⁶ Two glissile TDs can glide and react with each other when the angle between their Burger vectors is 60° , and they are within the capture radius R of each other.^{27,28} Because the reaction between glissile TDs raises the energy of the TDs, mobile TDs tend to glide to a lower energy state. The annealing at high temperature assists mobile TDs to move to equilibrium positions. Additionally, the rise in the vacancy achieved by the high-temperature annealing also increases the TD movement, which also drives mobile TDs to a lower energy state.²⁹ This implies that high-temperature annealing is very effective in reducing TDs. The TDD decreased dramatically in sample T_2 after TCA at 730°C compared with sample T_1 . At the same time, the

350 nm GaAs intermediate layer grown at 650°C avoided the decomposition of GaAs at the surface as well as contributed to the further reduction in TDDs. After that, the TDs were bent by the strain fields of the SLSs and propagated at the SLS interfaces along the $\langle 110 \rangle$ directions to meet and interact with each other.³⁰ The TCA at high temperature combined with SLSs reduced the defects through termination and bending.

To evaluate the effectiveness of the TCA and SLS dislocation filter, a structure of InP QD laser was grown on different GaAs/Si templates, and the same MDL structure was also grown on a native (001) GaAs substrate in the same run for a fair comparison. The detailed growth parameters of the laser have been reported in our previous publication.²² Figure 6 presents the RT photoluminescence (PL) spectra of the as-grown samples on the GaAs/Si templates and GaAs substrate excited by a 514 nm CW diode laser with a pump power of $2.5 \mu\text{W}$. The PL intensity of the InP QDs grown on the GaAs/Si templates increased with reduced TDD, indicating a better crystalline quality of the GaAs with TCA performed at a higher temperature. The residual tensile strain and the thermal mismatch between the III-V material and Si could have resulted in the red-shifted PL peak wavelength of the QDs grown on the GaAs/Si templates.³¹ Moreover, the apparent shoulder of the spectra in the longer wavelength can be attributed to the size fluctuation of the QDs.^{32,33} In addition, the emission of the $(\text{Al}_{0.1}\text{Ga})_{0.52}\text{In}_{0.48}\text{P}/(\text{Al}_{0.55}\text{Ga})_{0.52}\text{In}_{0.48}\text{P}$ quantum well under pumping gave rise to a weaker PL peak near 645 nm.

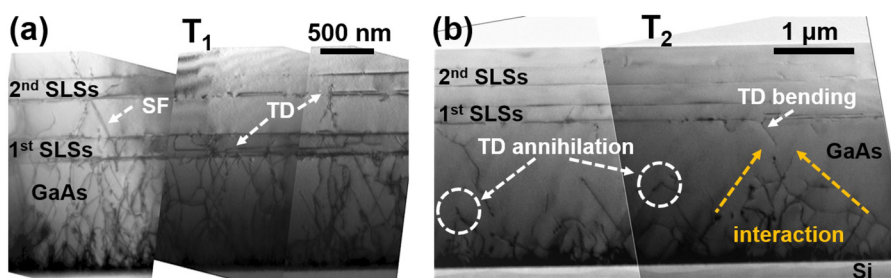


FIG. 5. X-TEM images of samples (a) T_1 and (b) T_2 , respectively. Some TDs and SFs could not be trapped by second SLSs in T_1 , while the interaction of defects took place obviously in GaAs epilayer of T_2 due to the higher annealing temperature.

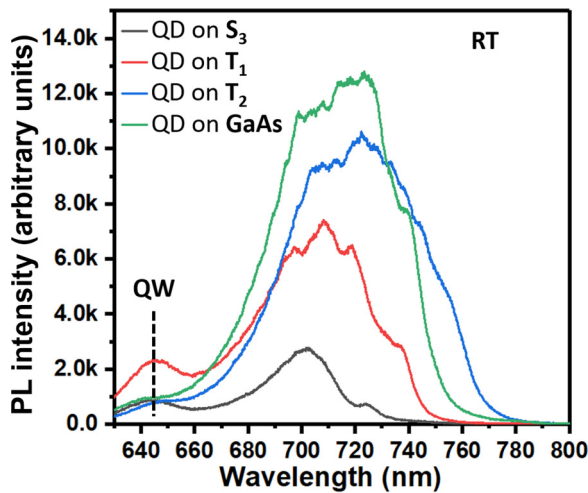


FIG. 6. RT-PL spectra of the InP QDs grown on the native GaAs and the different GaAs/Si templates pumped at 2.5 μW. PL intensity of the QDs on the GaAs/Si templates increased with the decrease in defect density.

MDLs with 1.5 μm-diameter were fabricated using a colloidal lithography method.³⁴ ICP etching was performed to define a region of cylindrical pillars on the samples, followed by selective wet etching to form AlGaAs pillars. For characterization, the

fabricated MDLs were optically pumped at RT using a CW 514 nm laser with a focused spot size of ~2 μm. Figures 7(a) and 7(b) show the representative power-dependent spectra of the MDLs grown on sample T₂ and the native GaAs substrate, respectively. The two sets of spectra show the transition from the spontaneous emission at an extremely low pumping power of 15 nW to the stimulated emission mode above the threshold (~1 μW). The image shown in the inset of Fig. 7(a) is a 70° tilted scanning electron microscope (SEM) image of a fabricated MDL on the GaAs/Si templates. Figure 7(c) displays the integrated output intensity plotted as a function of the pump power (L-L curve) of the representative MDLs on the GaAs substrate and the different GaAs/Si templates. Since the data measured at the region of spontaneous emission are dense, the X-axis is divided into two parts (-0.1-0.6 and 0.7-16 μW). Compared to the MDLs grown on sample S₃, the slope efficiency extracted from the linear region of the L-L curve of the MDLs grown on the other templates (T₁ and T₂) is larger, with a higher output intensity under the same pumping conditions. This indicates that the performance of the MDLs is related to the quality of the GaAs. Additionally, the lasing threshold and slope efficiency of the MDLs on sample T₂ are comparable to those on the native GaAs. The statistical data of the MDLs grown on the GaAs/Si templates and the native GaAs are summarized in Fig. 7(d) for a fair comparison. With the decrease in TDD in GaAs/Si templates, the average threshold is counted to be 1.76 μW for the MDLs on sample S₃, while gradually decreased to 1.16 μW for lasers on sample T₂ with the lowest TDD, the value of which is quite close to 1.07 μW on the native GaAs. The lasing thresholds of the MDLs on sample T₂,

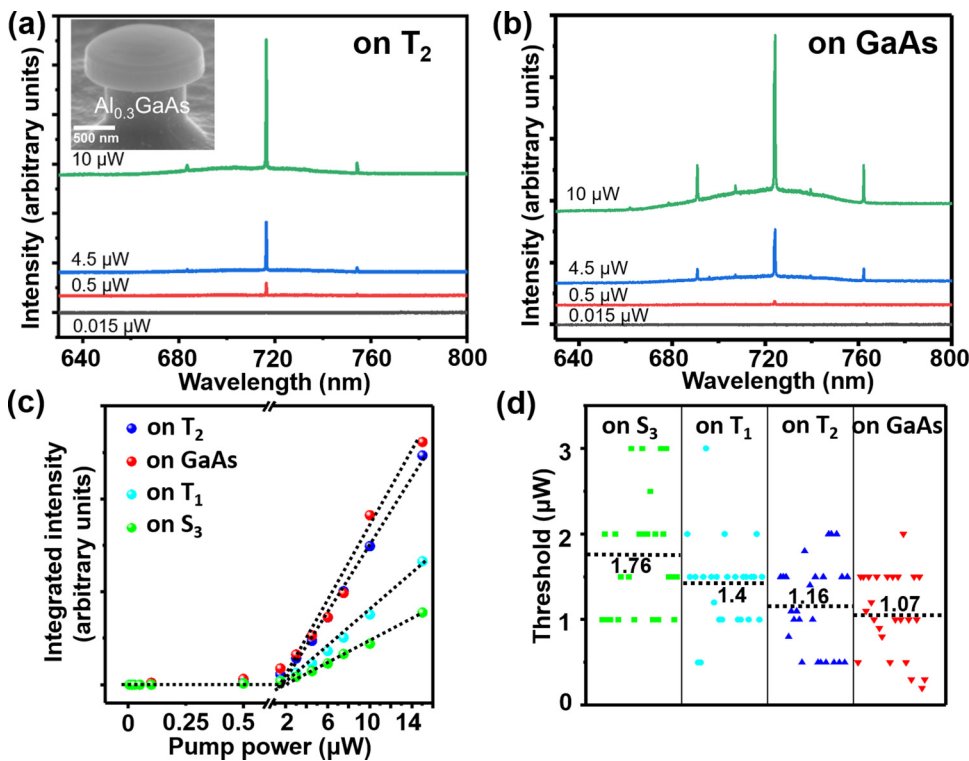


FIG. 7. Representative RT power-dependent PL spectra of InP QD MDLs grown on (a) sample T₂ and (b) the GaAs substrate, showing the emission intensities from spontaneous emission mode to lasing mode. Inset: SEM image of a fabricated 1.5 μm-diameter MDL. (c) L-L curves of MDLs on the GaAs substrate and the different GaAs/Si templates. The slope efficiency of MDLs on native GaAs and template T₂ is comparable. (d) Thresholds of the MDLs on the GaAs substrate and the GaAs/Si templates. The average threshold of MDLs on T₂ (1.16 μW) is comparable to that on GaAs substrate (1.07 μW).

clustering around $0.5\text{--}2\ \mu\text{W}$, are also comparable to those on the native GaAs substrate. We can ascribe the small difference in average threshold between the MDLs on sample T_2 ($1.16\ \mu\text{W}$) and the GaAs substrate ($1.07\ \mu\text{W}$) to the high quality of the GaAs/Si template as well as the InP QD gain material.

IV. CONCLUSIONS

In conclusion, we presented the growth of GaAs films on (001) Si substrates and investigated the effects of TCA and InGaAs/GaAs SLS buffers on the dislocation and morphology evolution of GaAs/Si templates. A smooth surface was obtained, thanks to an intermediate layer of GaAs deposited at $650\ ^\circ\text{C}$. PV-TEM measurements illustrated that the defect density in the optimized GaAs/Si templates is $1.4 \times 10^7\ \text{cm}^{-2}$. Based on the optimized GaAs/Si templates, we demonstrated InP QD MDLs with the lowest threshold of $0.5\ \mu\text{W}$ under CW optical pumping at RT. Furthermore, the performance of MDLs on the optimized GaAs/Si templates was comparable to that of MDLs on the native GaAs substrate, denoting the high material quality of the GaAs/Si template and smooth surfaces. We believe that the realization of superior performance of the MDLs grown on Si is a promising step toward the integration of Si photonics with optoelectronic devices.

SUPPLEMENTARY MATERIAL

See the [supplementary material](#) for the *in-situ* reflectance of sample S_1 and second TCA in S_3 and sample T_2 . X-TEM images of S_2 can also be found in this part.

ACKNOWLEDGMENTS

This work was supported by the Innovation and Technology Fund (No. ITS/201/19FP). The authors would like to thank the Material Characterization & Preparation Facility (MCPF) and the Nanosystem Fabrication Facility (NFF) of HKUST for their technical support.

AUTHOR DECLARATIONS

Conflict of Interest

The authors have no conflicts to disclose.

Author Contributions

J. Huang and Q. Lin contributed equally to this work.

Jie Huang: Writing – original draft (equal). **Qi Lin:** Writing – review and editing (equal). **Wei Luo:** Writing – review and editing (equal). **Liyang Lin:** Writing – review & editing (equal). **Kei May Lau:** Supervision (equal); Writing – review & editing (equal).

DATA AVAILABILITY

The data that support the findings of this study are available from the corresponding author upon reasonable request.

REFERENCES

¹Q. Li and K. M. Lau, *Prog. Cryst. Growth Charact. Mater.* **63**, 105 (2017).

- ²D. Thomson, A. Zilkie, J. E. Bowers, T. Komljenovic, G. T. Reed, L. Vivien, D. Marris-Morini, E. Cassan, L. Virot, J. M. Fédéli, J. M. Hartmann, J. H. Schmid, D. X. Xu, F. Boeuf, P. O'Brien, G. Z. Mashanovich, and M. Nedeljkovic, *J. Opt.* **18**, 073003 (2016).
- ³Y. T. Sun, C. Junesand, W. Metaferia, H. Kataria, N. Julian, J. Bowers, G. Pozina, L. Hultman, and S. Lourduos, *J. Appl. Phys.* **117**, 215303 (2015).
- ⁴C. Hantschmann, Z. Liu, M. Tang, S. Chen, A. J. Seeds, H. Liu, I. H. White, and R. V. Pentyl, *J. Lightwave Technol.* **38**, 4801 (2020).
- ⁵J. C. Norman, D. Jung, Y. Wan, and J. E. Bowers, *APL Photonics* **3**, 030901 (2018).
- ⁶J. Xu, Y. Song, X. Yu, A. Lin, M. Kong, J. Han, and N. Deng, *Opt. Express* **24**, 8097 (2016).
- ⁷R. Fekrazad, A. Sarrafzadeh, K. A. M. Kalhori, I. Khan, P. R. Arany, and A. Giubellino, *Photochem. Photobiol.* **94**, 775 (2018).
- ⁸Z. Li, C. P. Allford, S. Shutts, A. F. Forrest, R. Alharbi, A. B. Krysa, M. A. Cataluna, and P. M. Smowton, *IEEE Photonics Technol. Lett.* **32**, 1073 (2020).
- ⁹H. Kataria, W. Metaferia, C. Junesand, C. Zhang, N. Julian, J. E. Bowers, and S. Lourduos, *IEEE J. Sel. Top. Quantum Electron.* **20**, 380 (2014).
- ¹⁰L. Yang, M. T. Bulsara, K. E. Lee, and E. A. Fitzgerald, *J. Cryst. Growth* **324**, 103 (2011).
- ¹¹C. Merckling, N. Waldron, S. Jiang, W. Guo, N. Collaert, M. Caymax, E. Vancoille, K. Barla, A. Thean, M. Heyns, and W. Vandervorst, *J. Appl. Phys.* **115**, 023710 (2014).
- ¹²B. Shi, Q. Li, Y. Wan, K. W. Ng, X. Zou, C. W. Tang, and K. M. Lau, *IEEE Photonics Technol. Lett.* **27**, 748 (2015).
- ¹³Q. Li, K. W. Ng, C. W. Tang, K. M. Lau, R. Hill, and A. Vert, *J. Cryst. Growth* **405**, 81 (2014).
- ¹⁴K. Samonji, H. Yonezu, Y. Takagi, K. Iwaki, N. Ohshima, J. K. Shin, and K. Pak, *Appl. Phys. Lett.* **69**, 100 (1996).
- ¹⁵R. Alcotte, M. Martin, J. Moeyaert, R. Cipro, S. David, F. Bassani, F. Ducroquet, Y. Bogumilowicz, E. Sanchez, Z. Ye, X. Y. Bao, J. B. Pin, and T. Baron, *APL Mater.* **4**, 046101 (2016).
- ¹⁶Y. Ababou, P. Desjardins, A. Chenouf, R. Leonelli, D. Hetherington, A. Yelon, G. L'Espérance, and R. A. Masut, *J. Appl. Phys.* **80**, 4997 (1996).
- ¹⁷D. Jung, P. G. Callahan, B. Shin, K. Mukherjee, A. C. Gossard, and J. E. Bowers, *J. Appl. Phys.* **122**, 225703 (2017).
- ¹⁸Y. Takano, M. Hisaka, N. Fujii, K. Suzuki, K. Kuwahara, and S. Fuke, *Appl. Phys. Lett.* **73**, 2917 (1998).
- ¹⁹K. Li and W. Wang, *J. Cryst. Growth* **496–497**, 31 (2018).
- ²⁰K. Li, W. Wang, Q. Wang, and J. Leng, *J. Alloys Compd.* **768**, 74 (2018).
- ²¹B. Shi and J. Klamkin, *J. Appl. Phys.* **127**, 033102 (2020).
- ²²W. Luo, L. Lin, J. Huang, Y. Han, and K. M. Lau, *Opt. Lett.* **46**, 4514 (2021).
- ²³C. Shang, J. Selvidge, E. Hughes, J. C. Norman, A. A. Taylor, A. C. Gossard, K. Mukherjee, and J. E. Bowers, *Phys. Status Solidi A* **218**, 2000402 (2021).
- ²⁴M. Yamaguchi, A. Yamamoto, M. Tachikawa, Y. Itoh, and M. Sugo, *Appl. Phys. Lett.* **53**, 2293 (1988).
- ²⁵S. Farrell, M. V. Rao, G. Brill, Y. Chen, P. Wijewarnasuriya, N. Dhar, D. Benson, and K. Harris, *J. Electron. Mater.* **40**, 1727 (2011).
- ²⁶S. F. Fang, K. Adomi, S. Iyer, H. Morkoc, H. Zabel, C. Choi, and N. Otsuka, *J. Appl. Phys.* **68**, R31 (1990).
- ²⁷T. Ward, A. M. Sánchez, M. Tang, J. Wu, H. Liu, D. J. Dunstan, and R. Beanland, *J. Appl. Phys.* **116**, 063508 (2014).
- ²⁸B. Shi, Q. Li, and K. M. Lau, *J. Cryst. Growth* **464**, 28 (2017).
- ²⁹G. Wang, R. Loo, E. Simoen, L. Souriau, M. Caymax, M. M. Heyns, and B. Blanpain, *Appl. Phys. Lett.* **94**, 102115 (2009).
- ³⁰N. A. El-Masry, J. C. Tarn, and N. H. Karam, *J. Appl. Phys.* **64**, 3672 (1988).
- ³¹P. Dhingra, S. Fan, Y. Sun, R. D. Hool, B. Eng, and M. L. Lee, *Appl. Phys. Lett.* **117**, 181102 (2020).
- ³²Y. Wan, Q. Li, A. Y. Liu, A. C. Gossard, J. E. Bowers, E. L. Hu, and K. M. Lau, *Opt. Lett.* **41**, 1664 (2016).
- ³³B. Shi, S. Zhu, Q. Li, C. W. Tang, Y. Wan, E. L. Hu, and K. M. Lau, *Appl. Phys. Lett.* **110**, 121109 (2017).
- ³⁴L. Lin, Y. Xue, J. Li, W. Luo, J. Huang, and K. M. Lau, *Opt. Lett.* **46**, 2836 (2021).